A long Chandra HETGS observation of ζ Ori: an exemplary study of X-ray line profiles as wind mass loss diagnostics for OB stars

Maurice Leutenegger
D Cohen, M Gagné, J Hillier, S Owocki,
R Puebla, J Sundqvist, J Zsargó

Mass loss rates are very important

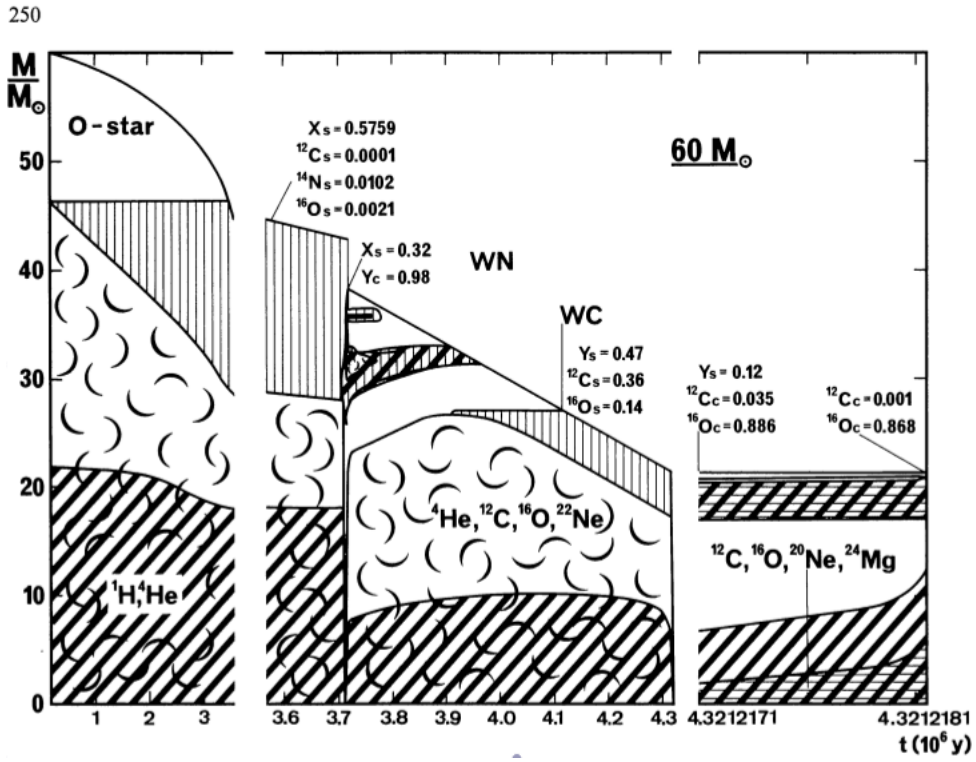

Meynet & Maeder:
stellar evolution is influenced by mass loss

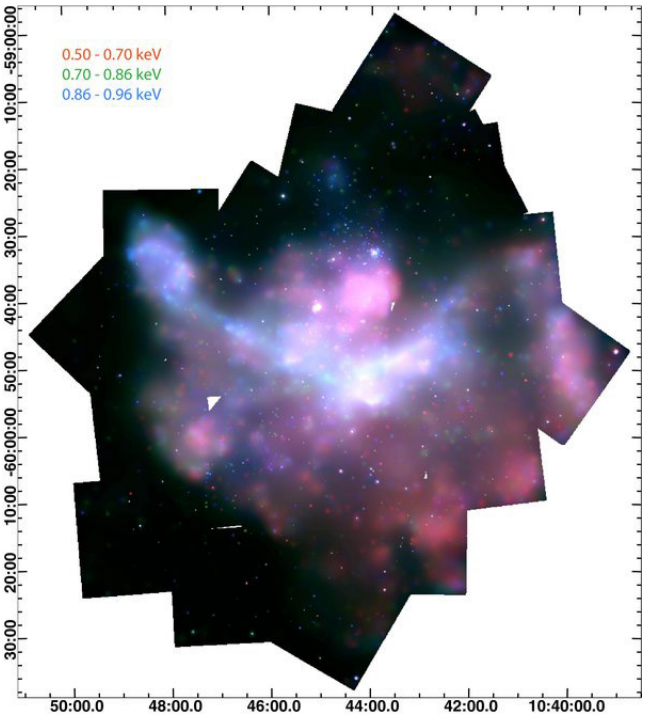

Townsley et al.: Carina nebula diffuse X-ray emission from hot gas heated by mechanical energy input from stellar winds

Optical/UV/IR/Radio diagnostics all have large systematic uncertainties

- Hα and radio free-free emission scale with density squared -> clumping
- UV resonance absorption lines depend on ion balance
- Even unsaturated UV resonance absorption lines from dominant ions may be affected by nonmonotonic velocity fields
- Systematics can be >~ factor of 3-10

Large discrepancy between UV resonance lines and radio/Hα

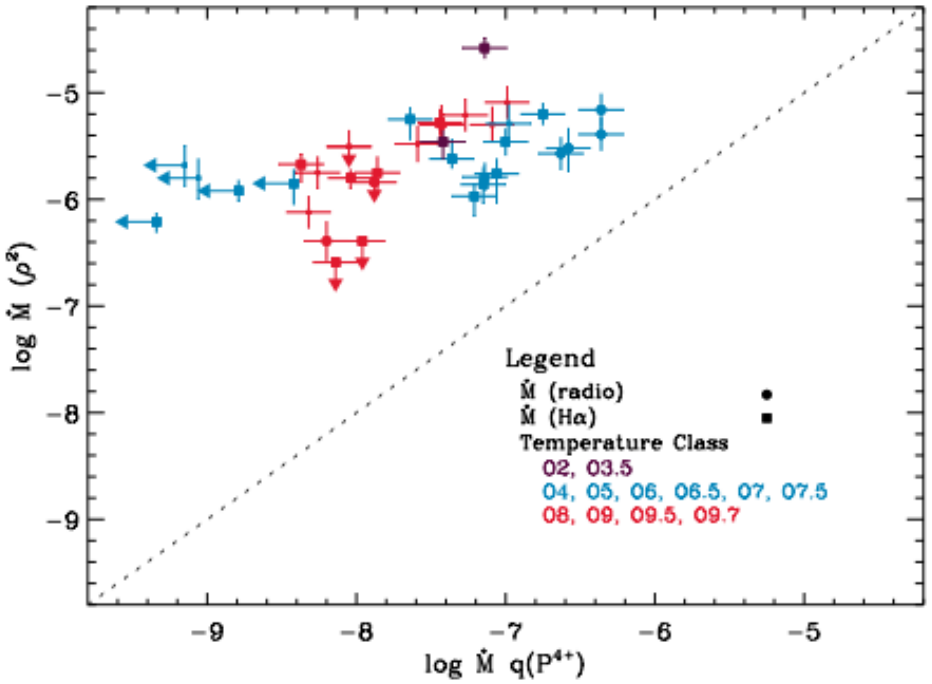

FIG. 3.—Comparison of $\dot{M}$ with $\dot{M}q(P^{+4})$. The shapes of symbols distinguish radio (*circles*) and Hα (*squares*) measurements, while symbol size separates the primary (*large*) and secondary (*small*) samples. Upper limits on nondetections are indicated by arrows. Color coding divides the entire sample into early (O2, O3, O3.5), mid (O4–O7.5), and late O types (O8–O9.7). The dotted line denotes a 1:1 correlation between the two measurements.

Fullerton et al. 2006:
P V lines are not saturated,
indicate much lower mass loss rate

X-ray profile asymmetry measures wind optical depth

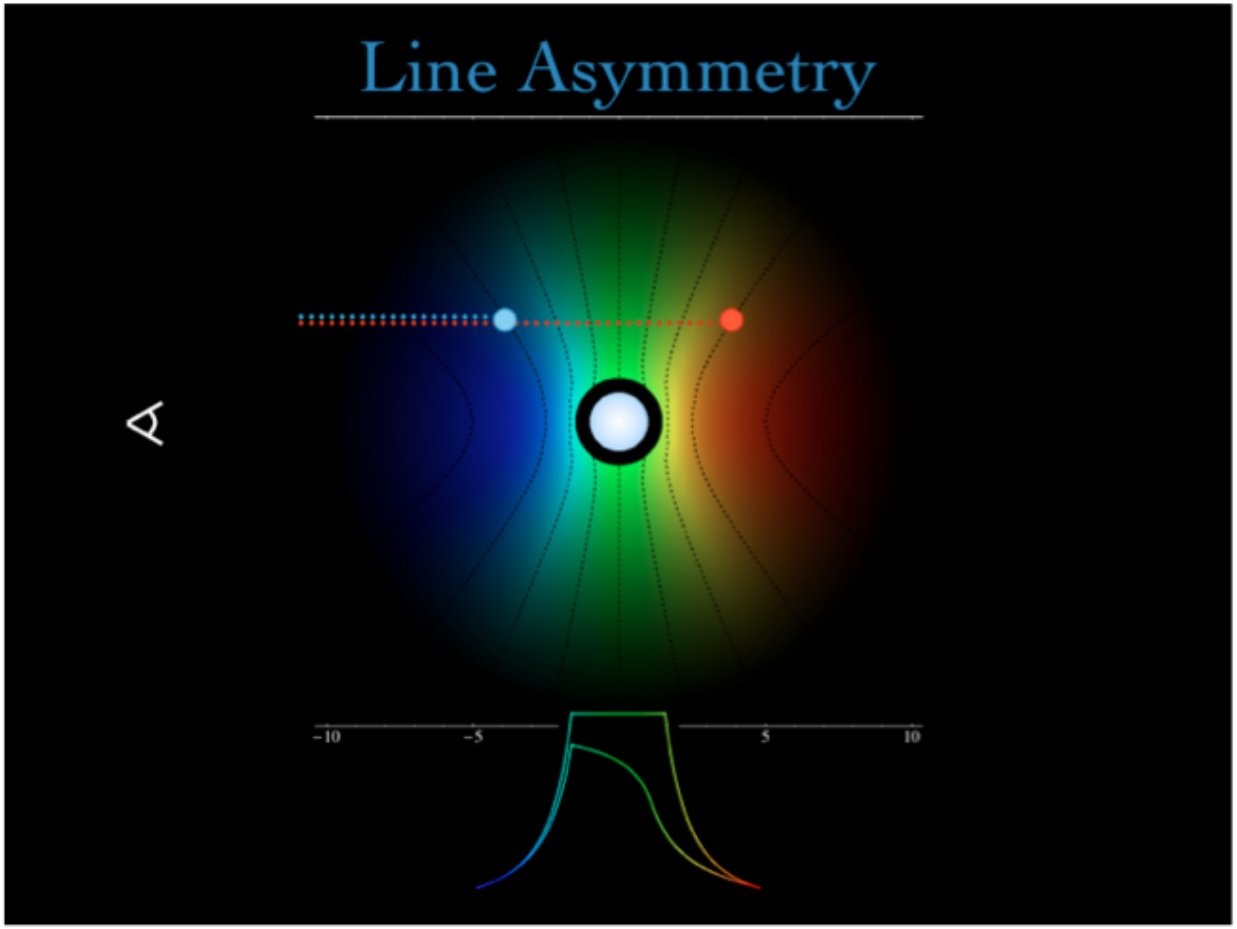

X-ray profile asymmetry measures wind optical depth τ_*

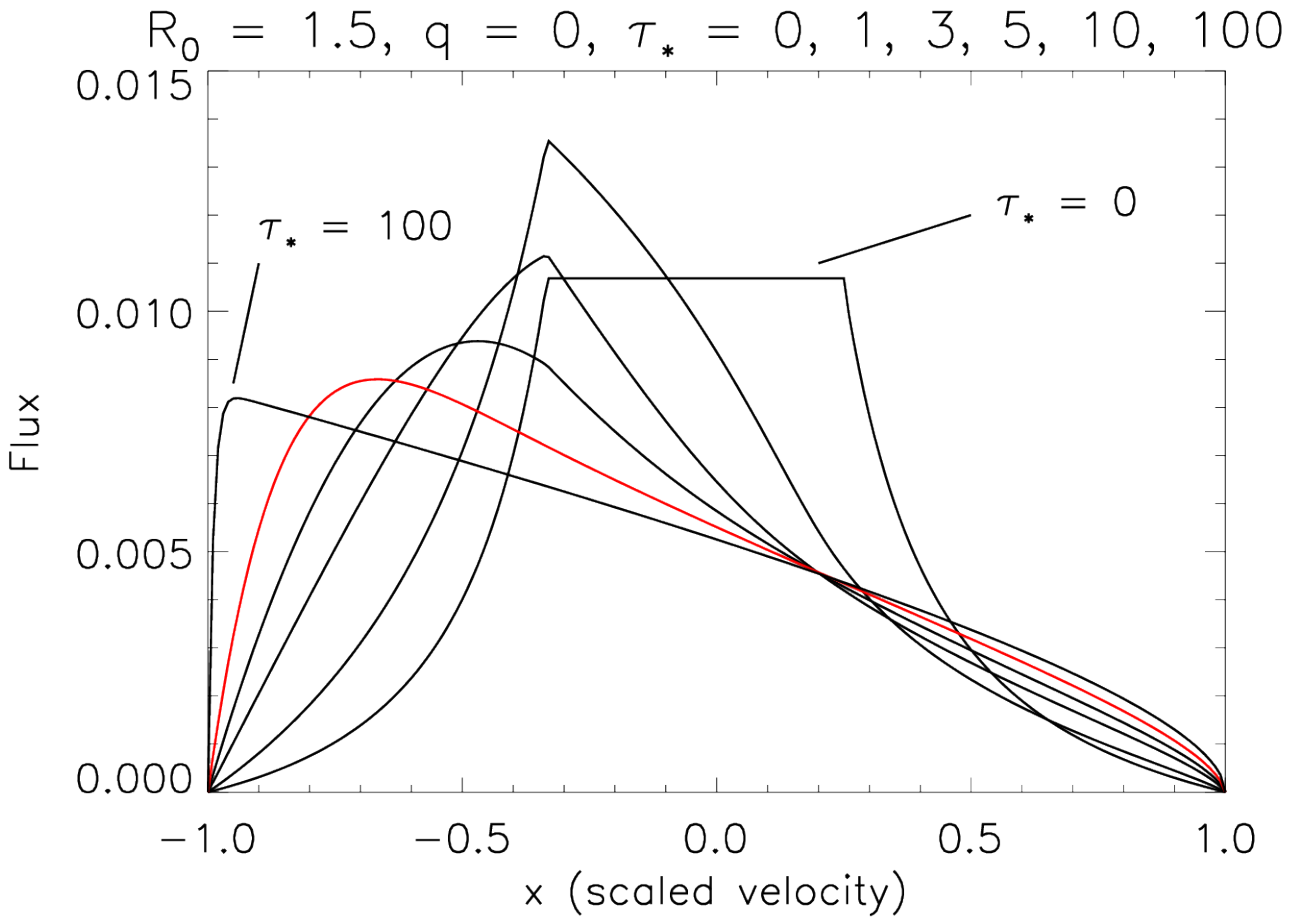

X-ray profile asymmetry measures wind optical depth τ_*

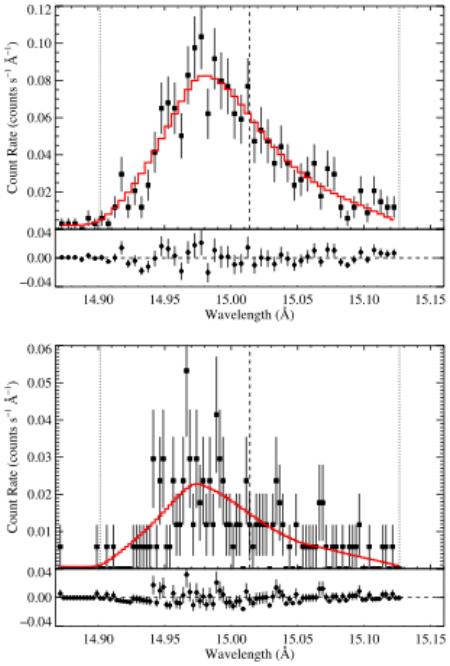

Figure 3. The Fe XVII line at 15.014 Å in the MEG (top) and HEG (bottom), with the best-fitting model superimposed. We have not done any rebinning of the data. The error bars represent Poisson, root-N, statistics. The dashed vertical lines indicate the laboratory rest wavelength of the emission line, and the two dotted vertical lines in each panel indicate the wavelengths associated with the Doppler shift due to the stellar wind terminal velocity of 2250 km s^{-1}. The model is shown as the thick (red) histogram, while the data are shown as (black) solid squares with error bars. The fit residuals are shown in the horizontal windows below the data, with the same one sigma error bars that are shown with the data.

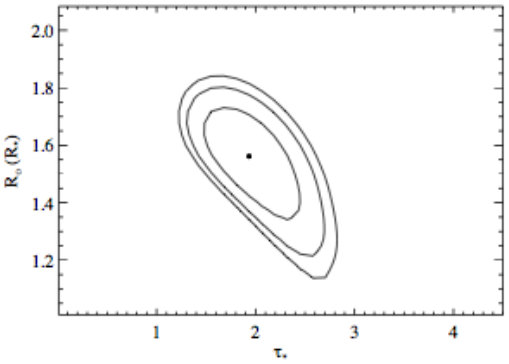

Figure 4. Confidence contours (68, 90, and 95 percent) for the model fitting of the the Fe XVII line at 15.014 Å. The best fit, shown in Fig. 3, is represented by the filled circle.

Cohen et al. 2010

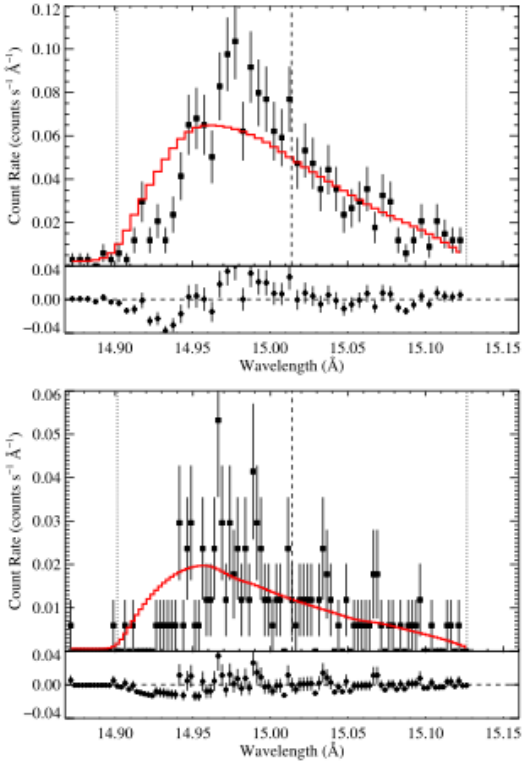

Figure 5. The Fe XVII line at 15.014 Å in the MEG (top) and HEG (bottom), with the best-fitting model having $\tau_* = 5.30$ superimposed. This is the value implied by the smooth-wind Hα mass-loss rate and our wind opacity model. The normalization and R_o were the adjustable parameters of this fit. Even this best-fitting model is statistically unacceptable.

Can do this for all lines

- Best fit for all lines in Chandra HETGS spectrum of ζ Pup
- τ^* is proportional to κ, $\dot{M}$
- Mass loss rate is reduced by factor of ~2.5

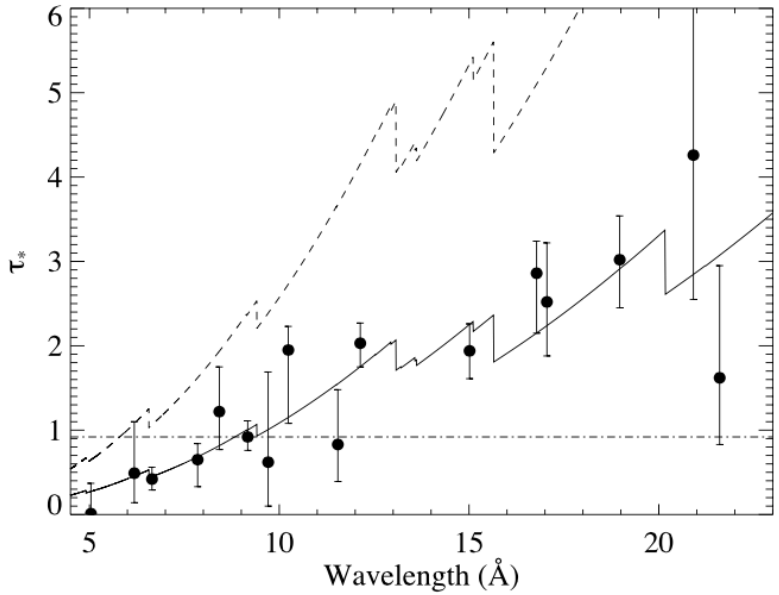

Cohen et al. 2010

Can apply same method to other stars

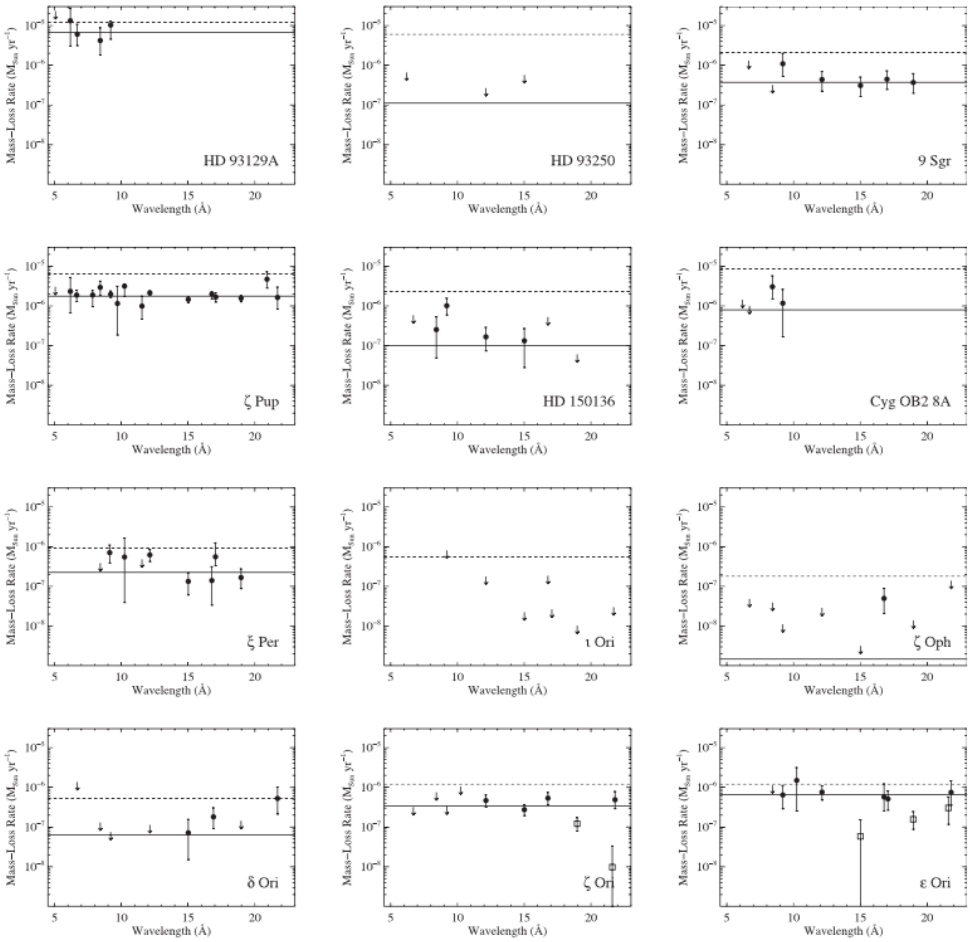

Cohen et al. 2014

Can apply same method to other stars

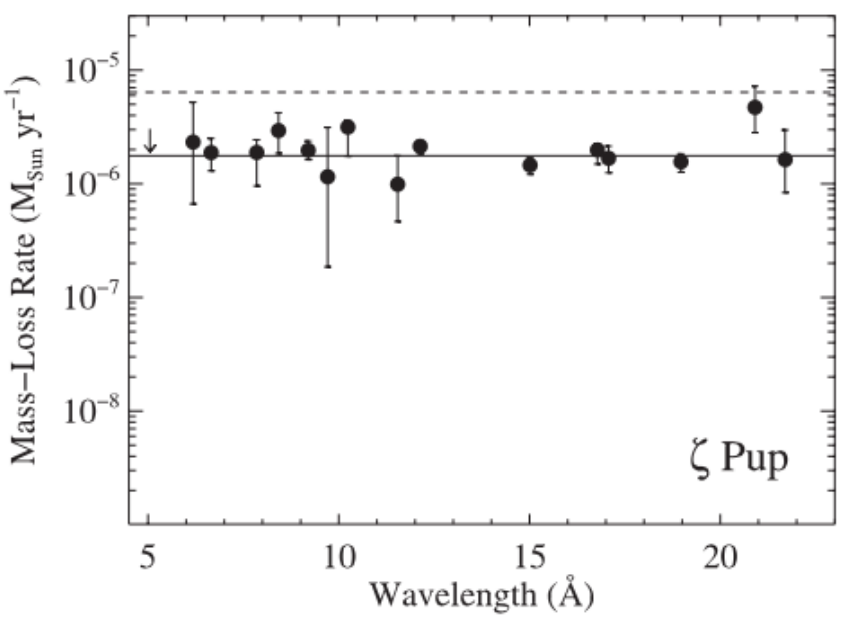

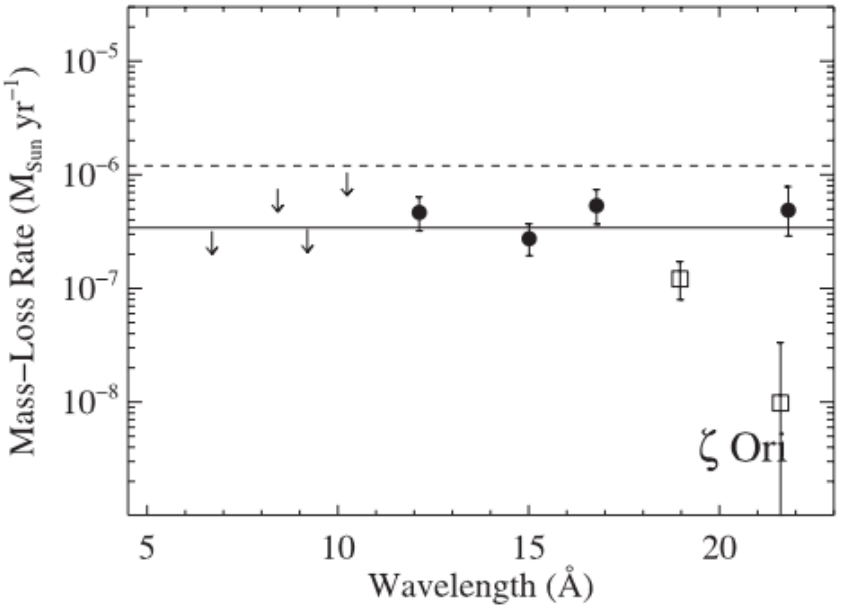

Cohen et al. 2014

Difficulties in X-ray mass-loss rate measurements

- small possible sample (N_H, d)
- many stars have low enough $\dot{M}$ that asymmetry is not very large
- weak asymmetry increases susceptibility to both statistical and systematic errors

ζ Ori is less asymmetric than ζ Pup

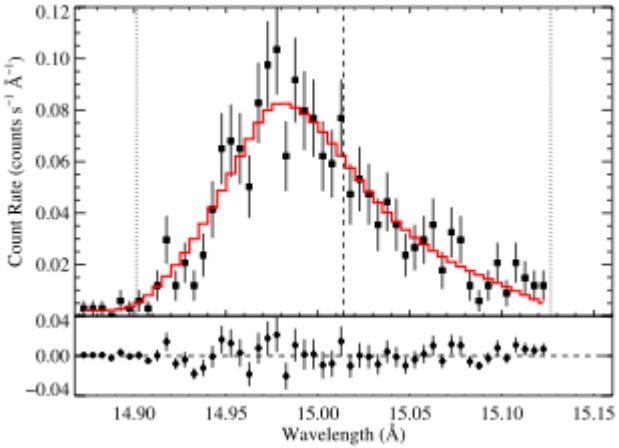

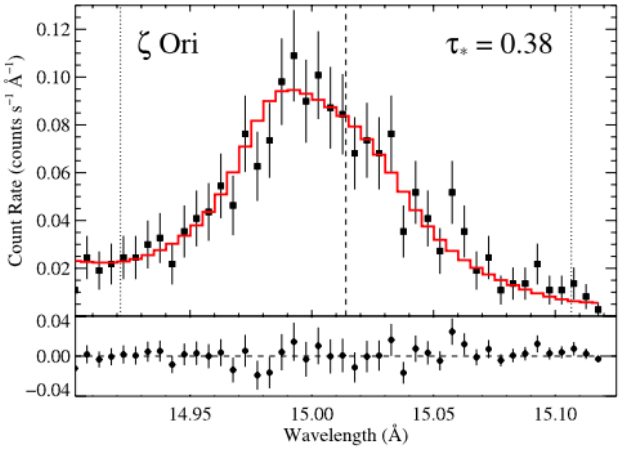

ζ Ori

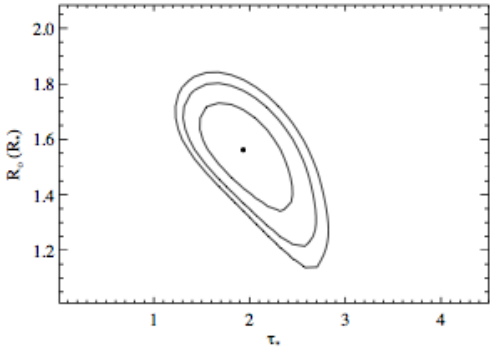

ζ Pup

Figure 4. Confidence contours (68, 90, and 95 percent) for the model fitting of the the Fe XVII line at 15.014 Å. The best fit, shown in Fig. 3, is represented by the filled circle.

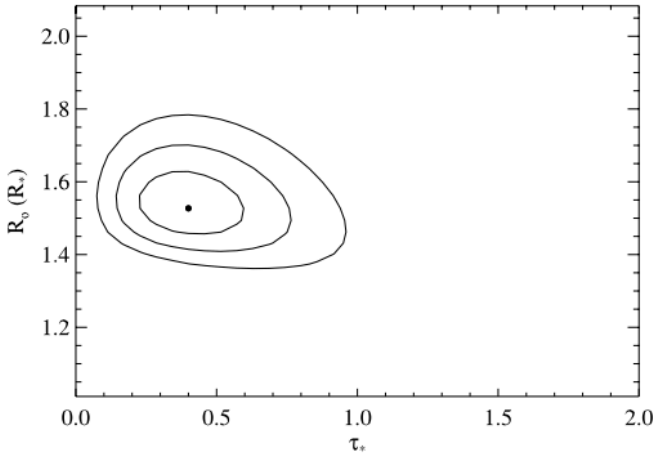

Possible systematics

- Instrument (wavelength scale)
- Radial velocity
- Companions (spectroscopic or visual binary)
  - CWB interactions?
- Wind and stellar parameter assumptions (velocity law – β, v_∞; R_*; d)
- Modeling uncertainties in κ
- Radiative transfer effects (porosity, resonance scattering, ...?)

ζ Ori B

- Known visual binary with separation 2.4”
- For LP observations, grating dispersion direction oriented to separate A and B in cross dispersion

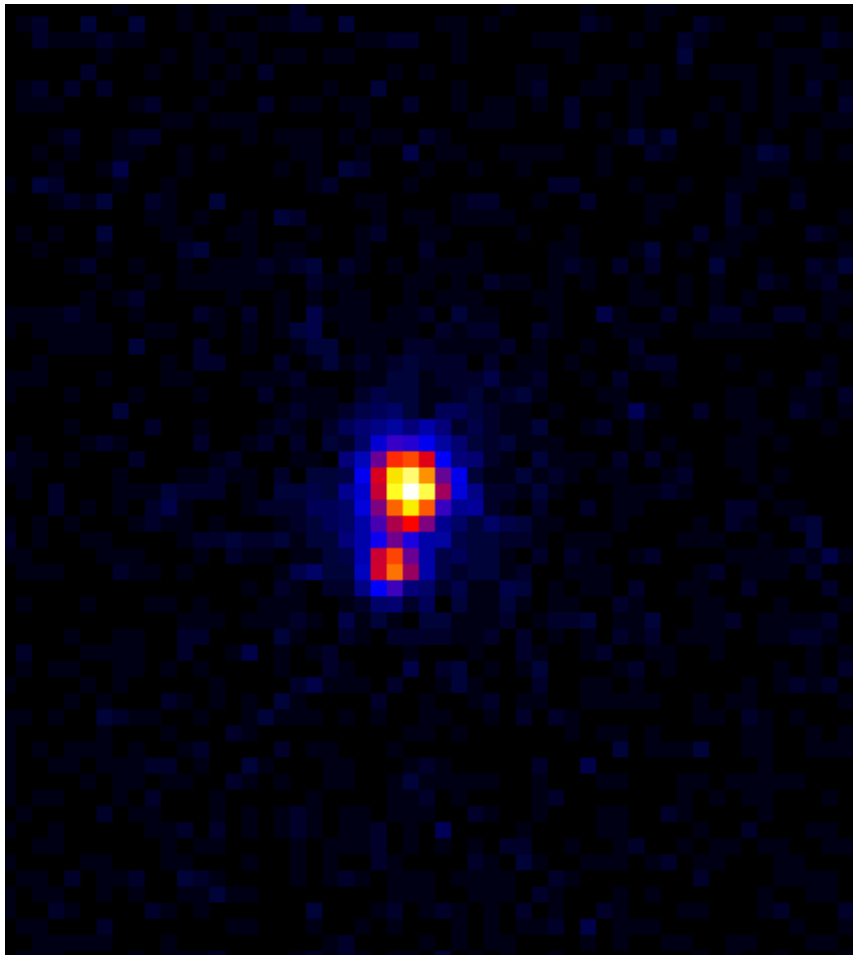

ζ Ori Ab

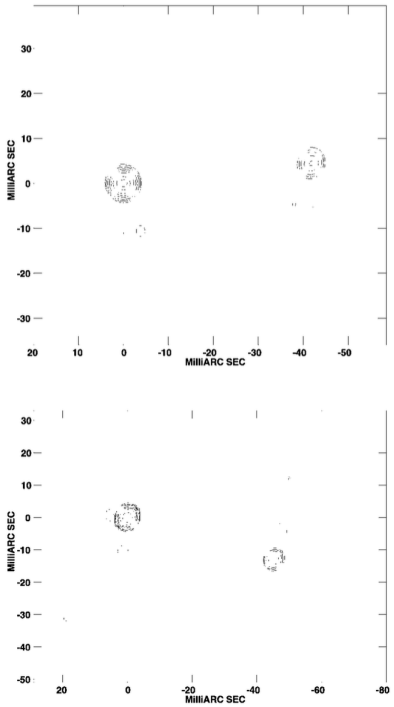

FIG. 1.—Maps of component A for 1998 February 12 (*top*) and 1999 February 23 (*bottom*). The contour levels are at −0.5, 0.5, 1, 2, 5, 10, 20, 50, and 80 percent of the peak. The restoring beam is circular with an FWHM of 3 mas.

From Hummel et al. (2000,2013)

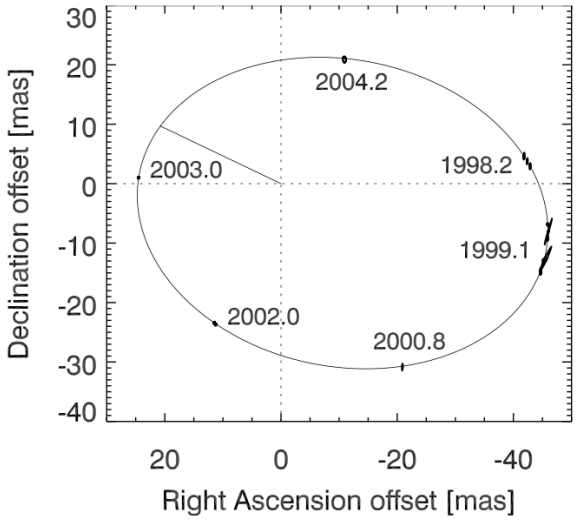

Fig. 4. Orbit of ζ Orionis Ab around Aa (center). The line indicates the secondary Ab at periastron. A few selected epochs are marked.

Table 4. Stellar parameters for the components of the ζ Ori system based on the photometric distance.

Parameter	Aa	Ab	B
Sp. type	O9.5 Iab	B1 IV	B0 III
m_V [mag]	2.1	4.3	4.0
M_V (photometry) [mag]	−6.0	−3.9	−4.1[a]
M_V (orbit) [mag]	−5.5	−3.3	−3.6
$M_\star$ [$M_\odot$]	33 ± 10	14 ± 3	–
$R_\star$ [$R_\odot$]	20.0 ± 3.2	7.3 ± 1.0	–

Notes. [(a)] Adopted (see text).

ζ Ori Ab

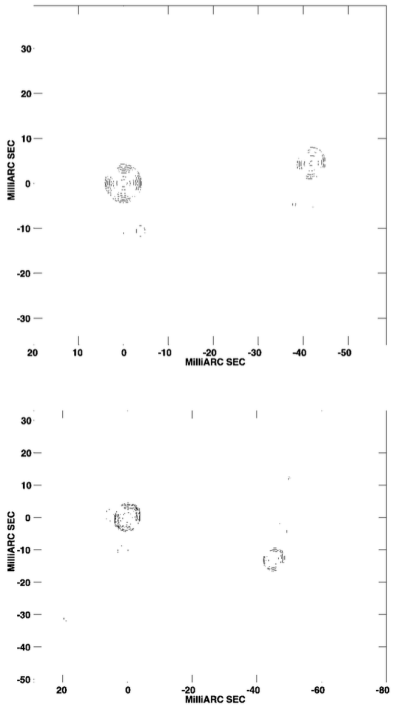

FIG. 1.—Maps of component A for 1998 February 12 (*top*) and 1999 February 23 (*bottom*). The contour levels are at −0.5, 0.5, 1, 2, 5, 10, 20, 50, and 80 percent of the peak. The restoring beam is circular with an FWHM of 3 mas.

From Hummel et al. (2000,2013)

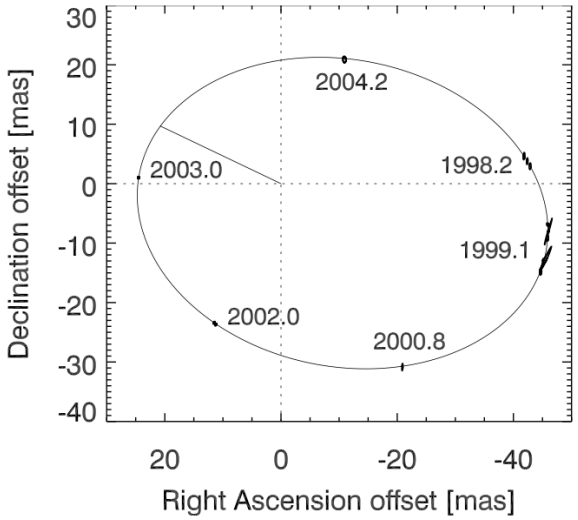

Fig. 4. Orbit of ζ Orionis Ab around Aa (center). The line indicates the secondary Ab at periastron. A few selected epochs are marked.

Table 4. Stellar parameters for the components of the ζ Ori system based on the photometric distance

Parameter	Aa	Ab	B
Sp. type	O9.5 Iab	B1 IV	B0 III
m_V [mag]	2.1	4.3	4.0
M_V (photometry) [mag]	−6.0	−3.9	−4.1[a]
M_V (orbit) [mag]	−5.5		−5.6
$M_\star$ [$M_\odot$]	33 ± 10	14 ± 3	–
$R_\star$ [$R_\odot$]	20.0 ± 3.2	7.3 ± 1.0	–

Notes. [(a)] Adopted (see text).

Compare ζ Ori A to ζ Ori B

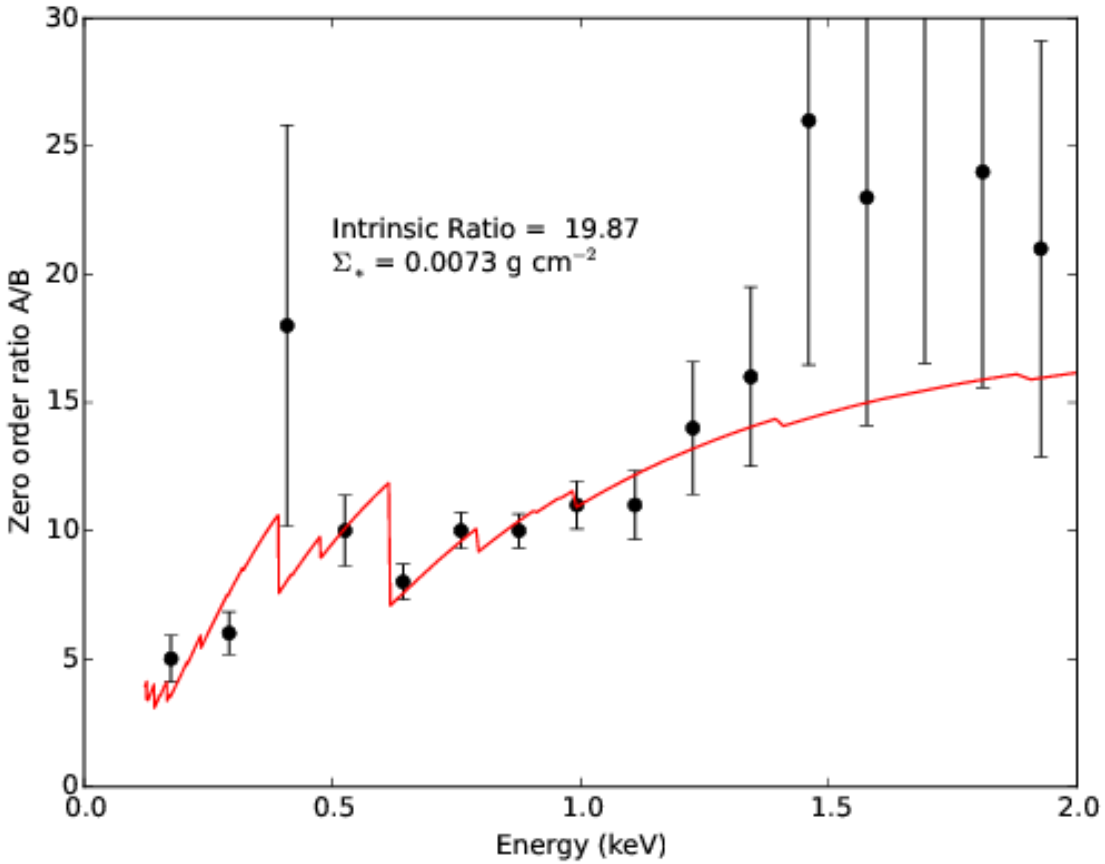

Model ζ Ori A including ζ Ori Ab

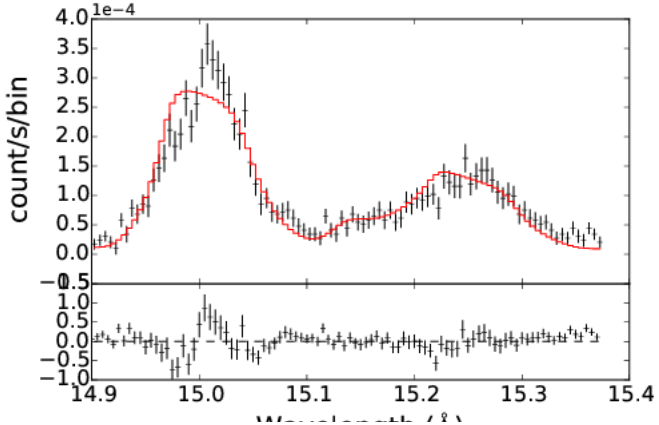

<- Single star ->

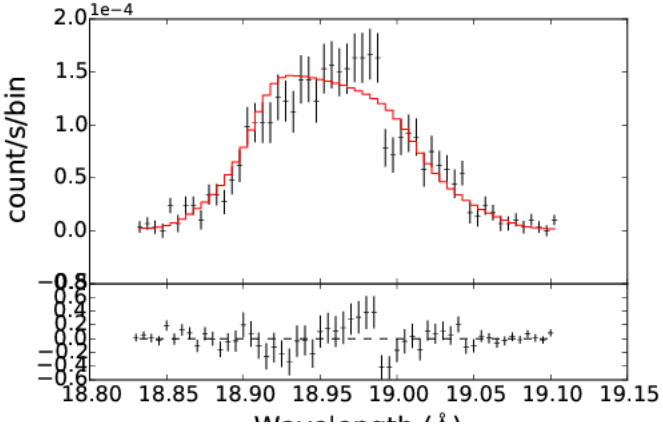

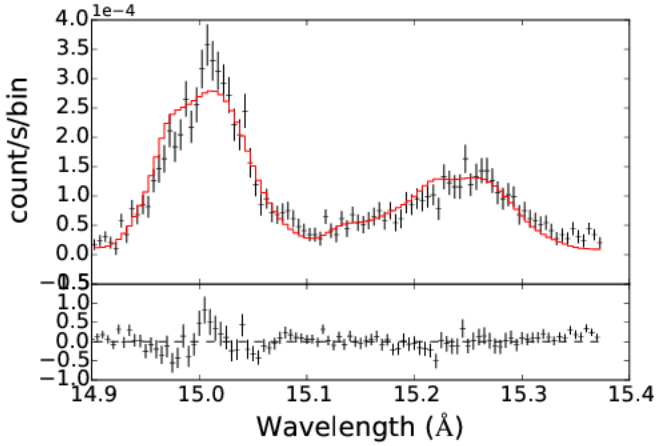

<- Includes Ab ->

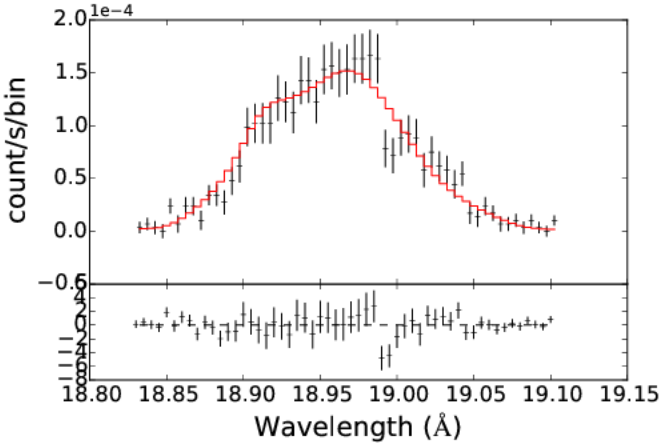

Fe XVII 3d-2p

O VIII Lyα

$\dot{M}$ is increased when Ab is included

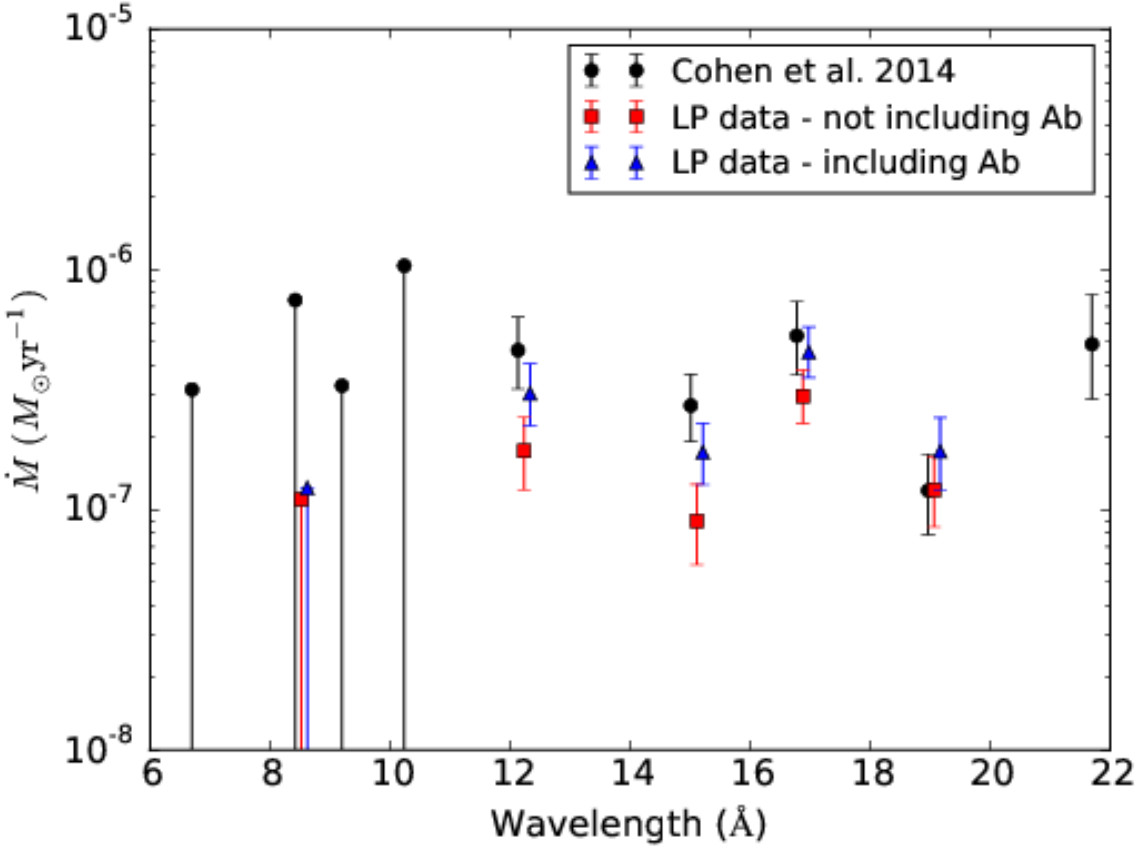

Porosity – reduction in effective optical depth due to large clumps

"Pancake" shaped clumps: anisotropic porosity

Feldmeier et al. 2003

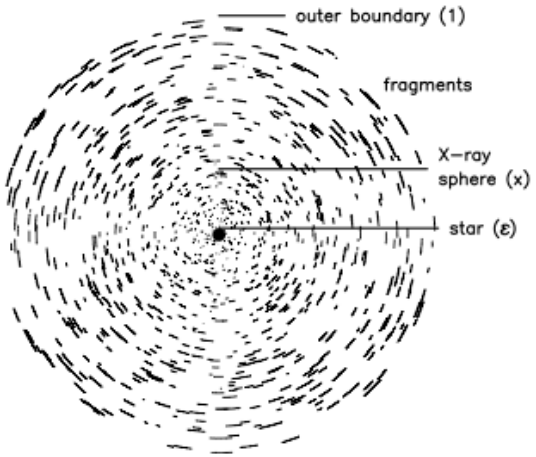

Fig. 1. Fragmented wind, with $N = 10$ fragments per radial ray. The symbols in brackets designate radii.

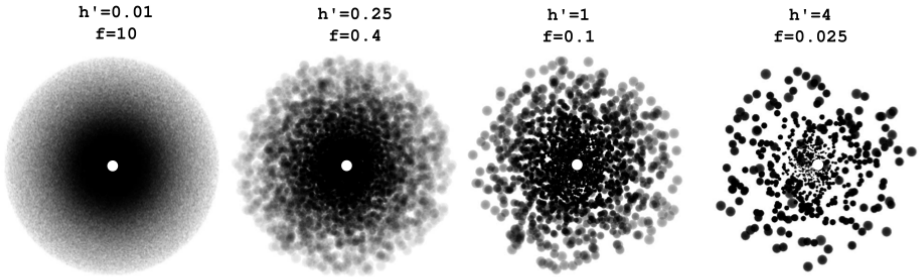

FIG. 3.—Explicit manifestation of clump structure in models set to have statistical properties corresponding to porosity length scale factors $h' = 1/100$, 1/4, 1, and 4. The individual clumps have a diameter that increases with radius as $\ell = 0.1r$, leading to radially-fixed volume filling factors $f = \ell'/h' = 10$, 0.4, 1, and 0.025, respectively. The leftmost panel, with the smallest porosity length, corresponds nearly to a completely smooth wind case. In each panel, the gray-scale level is proportional to the transmission of a uniform illumination from the back, i.e., as $\exp[-\tau]$, where τ is the integrated optical depth along any given line of sight. The optical thickness of individual clumps decreases outward, with an overall level corresponding to a total wind optical depth parameter $\tau_* = 5$. These visualizations assume that the viewer is at infinity, so the apparent size of each clump is proportional to its linear scale, without any perspective effect; clumps that appear smaller actually are smaller, because they are at smaller radii. For context, the central white disk illustrates the size and location of the central star, and for clarity, only clumps within the central 20 R_* are included.

"Ball" shaped clumps: isotropic porosity

Owocki & Cohen et al. 2006
(Fig. by R. Townsend)

Effects of porosity

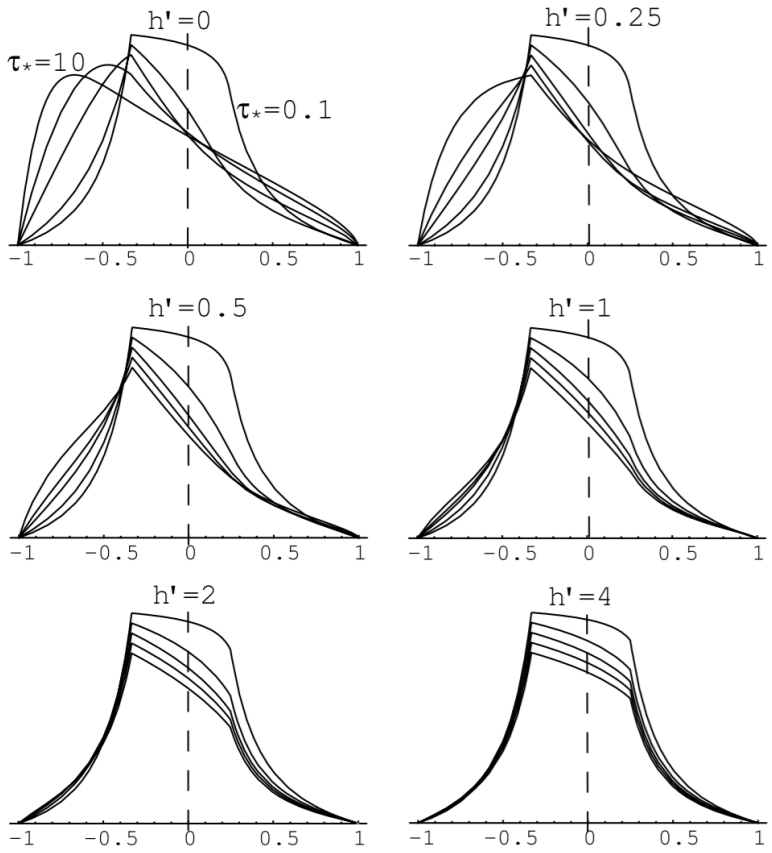

- Higher porosity leads to more symmetric profiles for the same mass-loss rate...
- or higher mass-loss rate for the same profile (shape is degenerate to zeroeth order)

Porosity is constrained

- Porosity lengths greater than ~ R_* are disfavored theoretically
- Also disfavored by HMXB variability studies (see e.g. talk and poster by V. Grinberg)
- Also disfavored by subtle changes in O star line profile shape not seen in high S/N data

Effect of iso porosity with $h_\infty = R_*$

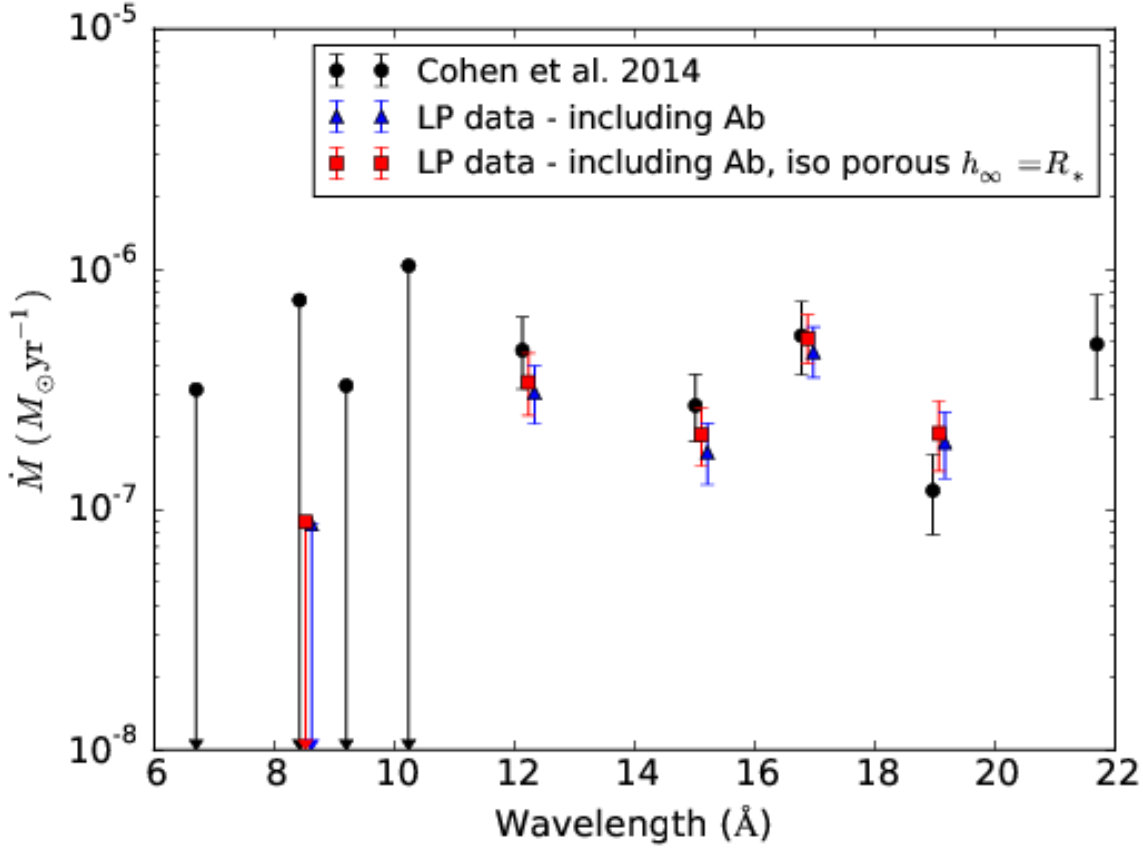

Resonance scattering

- Shown to be important in ζ Pup N VI and O VII
- Relies on local anisotropy in escape probability due to variation in line-of-sight velocity gradient
- Can symmetrize resonance lines, ignores non-resonance lines

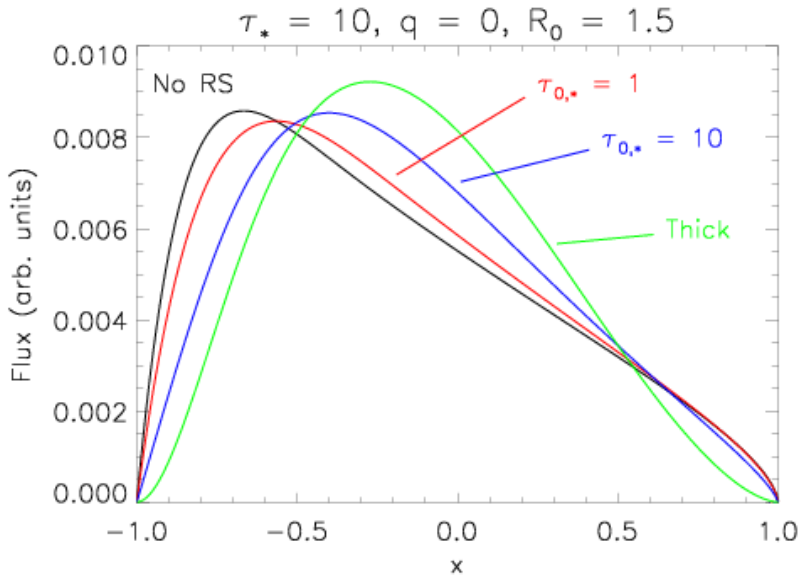

No resonance scattering in ζ Pup N VI

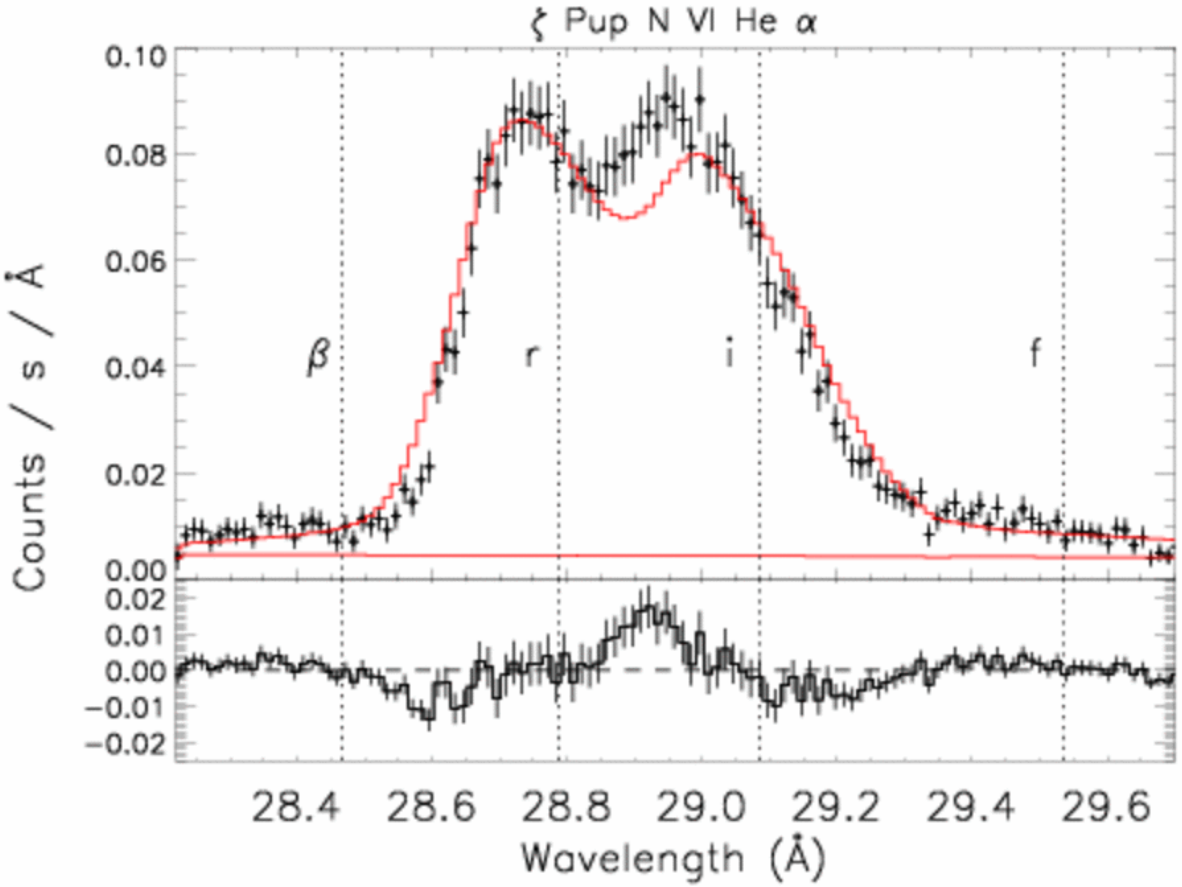

Resonance scattering in ζ Pup N VI!

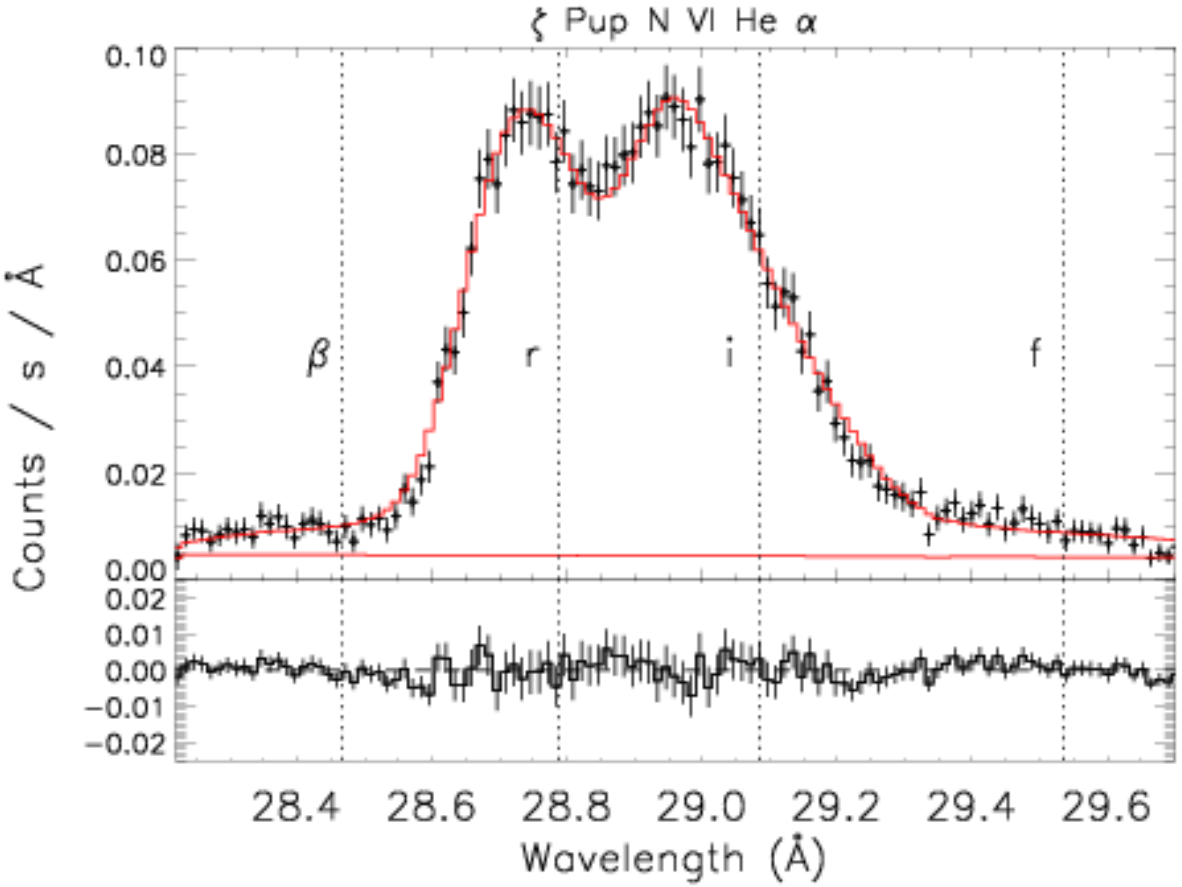

How about O VII in ζ Ori?

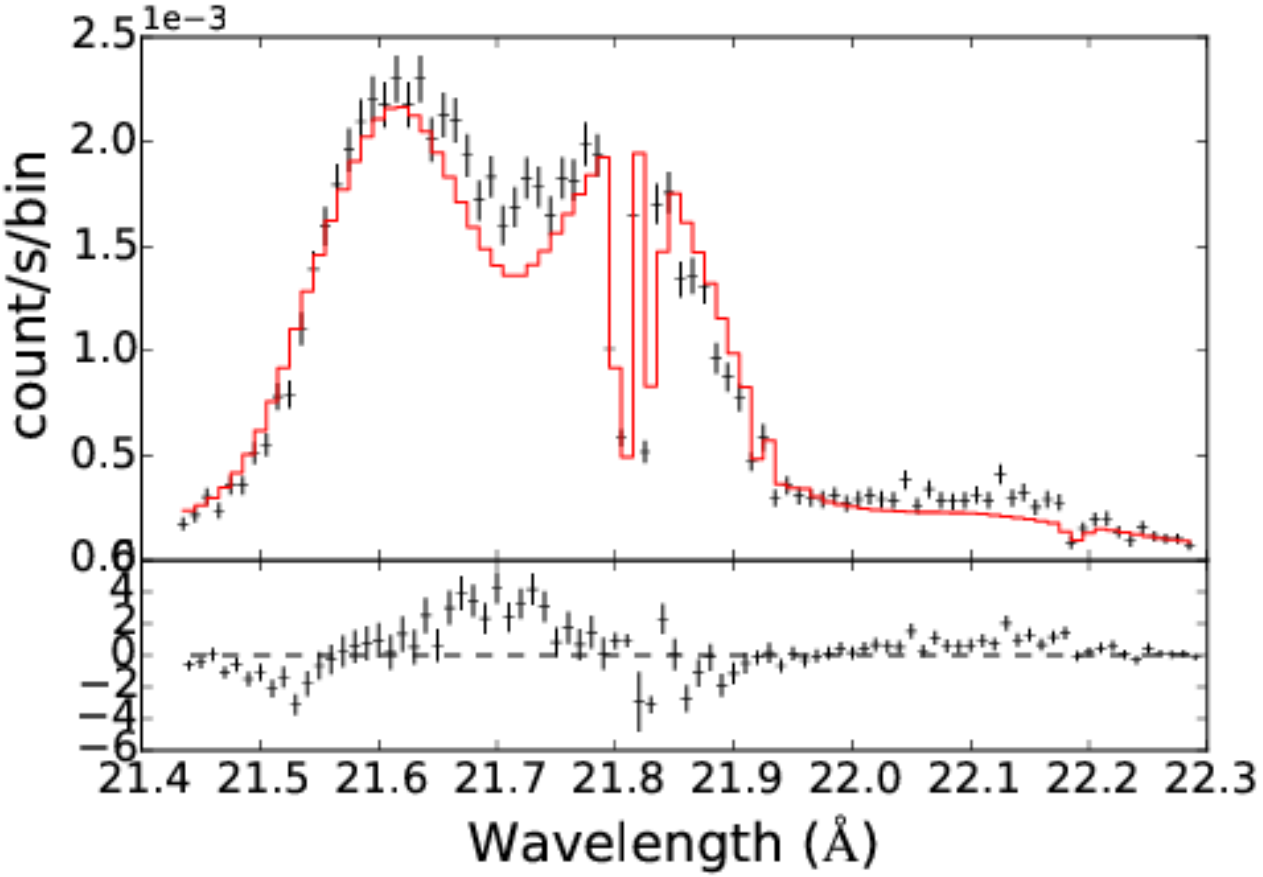

How about O VII in ζ Ori?

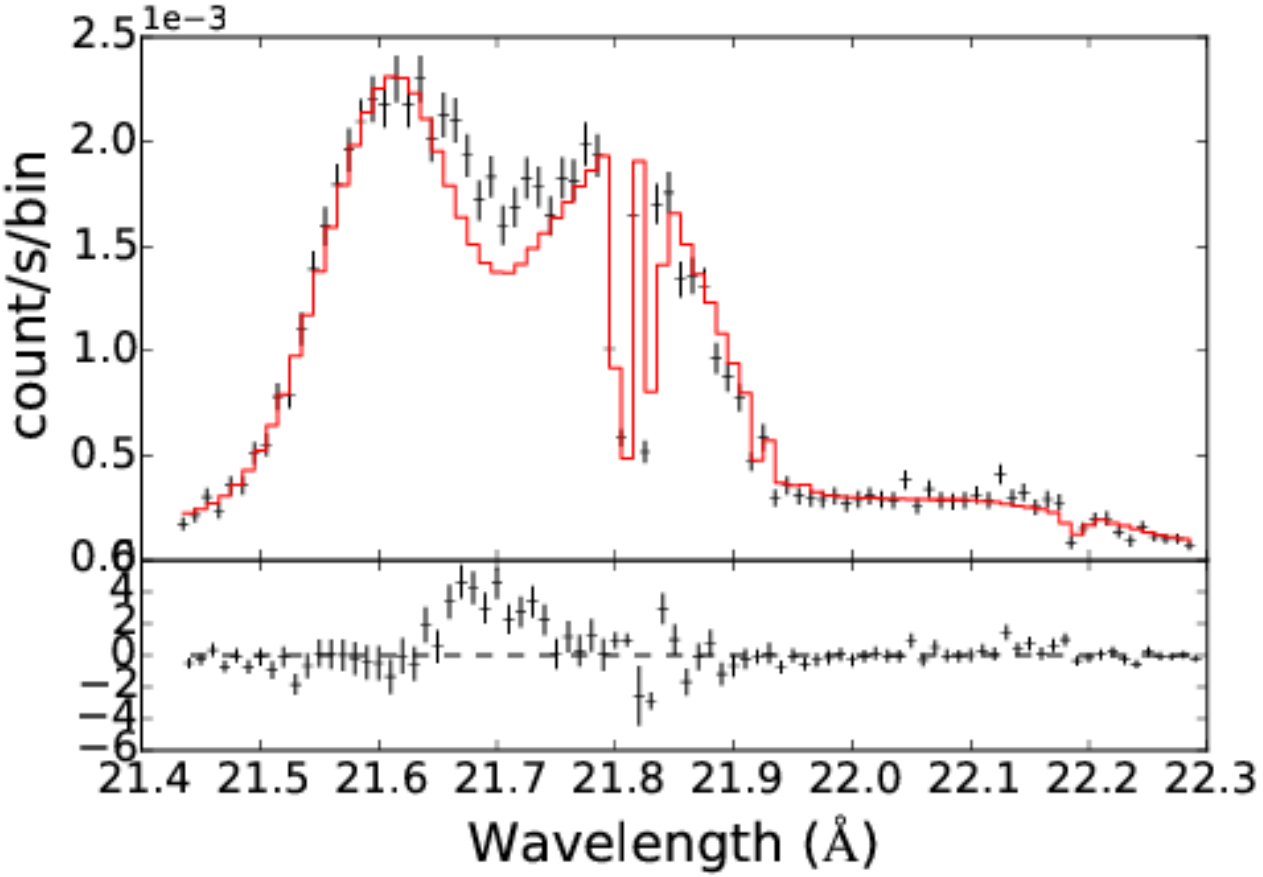

What is going on?

- Systematics in the data? or in modeling assumptions?
- Resonance scattering is more complicated than we thought?
- An unknown or unexpected line?
- Need to understand this before we can feel quantitatively confident in our interpretation

Summary (1/2)

- The X-ray lines of ζ Ori Aa are consistent with the emerging consensus of factor of few lower mass loss rates for O stars
- It's possible to make a relatively precise measurement of $\dot{M}$ with sufficient exposure time, but a detailed accounting of systematic effects is mandatory

Summary (2/2)

- Although we've made a lot of progress, there are still significant uncertainties in X-ray radiative transfer (porosity; resonance scattering) that require further exploration
- Even a limited sample has a big impact on the field because of the large systematic uncertainties on diagnostics in all wavelength bands

Backup slides

Moment analysis shows signficant skewness

Table 3. First and third moments of the emission-line profiles.

Ion	λ_o (Å)	M1	M1/uncert.	M3	M3/uncert.
O VIII	18.969	-0.0818 ± 0.0135	-6.08	7.9914 ± 4.8511	1.65
O VII	18.627	-0.1138 ± 0.0416	-2.74	4.5943 ± 2.9983	1.53
Fe XVII	16.780	-0.1652 ± 0.0229	-7.32	7.5967 ± 3.9259	1.94
O VIII	16.006	-0.0464 ± 0.0247	-1.88	3.9309 ± 3.8114	1.03
Fe XVII	15.014	-0.0792 ± 0.0173	-4.58	12.5198 ± 5.5363	2.26
Ne X	12.134	$-0.0801 \pm .0194$	-4.13	10.1529 ± 5.4936	1.85
Ne IX	11.544	-0.1108 ± 0.0368	-3.01	2.8778 ± 4.0377	0.71

Note: M1 and M3 are the first and third moments of the line profiles, respectively. The following columns show the ratio of the values of these moments, for the indicated unblended lines, to their formal uncertainties. We interpret the values in these columns as significance indicators of the first and third moments' deviation from zero, as described in Section 3.

Results for Zeta Ori Chandra HETGS observations, Cohen et al. 2006